ACS OMEGA

http://pubs.acs.org/journal/acsodf

Article

Bifunctional Ionic Deep Eutectic Electrolytes for CO_2 Electroreduction

Ahmed Halilu,* Mohamed Kamel Hadj-Kali,* Mohd Ali Hashim, Rozita Yusoff, and Mohamed Kheireddine Aroua

Cite This: *ACS Omega* 2022, 7, 37764−37773

Read Online

ACCESS | Metrics & More | Article Recommendations | Supporting Information

ABSTRACT: CO_2 is a low-cost monomer capable of promoting industrially scalable carboxylation reactions. Sustainable activation of CO_2 through electroreduction process (ECO_2R) can be achieved in stable electrolyte media. This study synthesized and characterized novel diethyl ammonium chloride−diethanolamine bifunctional ionic deep eutectic electrolyte (DEACl−DEA), using diethanolamine (DEA) as hydrogen bond donors (HBD) and diethyl ammonium chloride (DEACl) as hydrogen bond acceptors (HBA). The DEACl−DEA has −69.78 °C deep eutectic point and cathodic electrochemical stability limit of −1.7 V *versus* Ag/AgCl. In the DEACl−DEA (1:3) electrolyte, electroreduction of CO_2 to $CO_2^{\bullet-}$ was achieved at −1.5 V *versus* Ag/AgCl, recording a faradaic efficiency (FE) of 94%. After 350 s of continuous CO_2 sparging, an asymptotic current response is reached, and DEACl−DEA (1:3) has an ambient CO_2 capture capacity of 52.71 mol/L. However, DEACl−DEA has a low faradaic efficiency <94% and behaves like a regular amine during the CO_2 electroreduction process when mole ratios of HBA−HBD are greater than 1:3. The electrochemical impedance spectroscopy (EIS) and COSMO-RS analyses confirmed that the bifunctional CO_2 sorption by the DEACl−DEA (1:3) electrolyte promote the ECO_2R process. According to the EIS, high CO_2 coverage on the DEACl−DEA/Ag-electrode surface induces an electrochemical double layer capacitance (EDCL) of 3.15×10^{-9} F, which is lower than the 8.76×10^{-9} F for the ordinary DEACl−DEA/Ag-electrode. COSMO-RS analysis shows that the decrease in EDCL arises due to the interaction of CO_2 non-polar sites (0.314, 0.097, and 0.779 e/nm^2) with that of DEACl (0.013, 0.567 e/nm^2) and DEA (0.115, 0.396 e/nm^2). These results establish for the first time that a higher cathodic limit beyond the typical CO_2 reduction potential is a criterion for using any deep eutectic electrolytes for sustainable CO_2 electroreduction process.

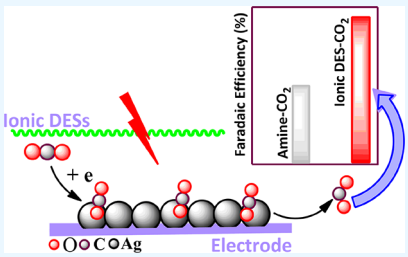

1. INTRODUCTION

The current level of CO_2 in the atmosphere is approximately 420.57 ppm, causing a rise in global temperature because CO_2 can absorb UV-radiation from the sun and emit heat, consequently causing significant climate change.[1−8] Therefore, sustainable CO_2 sequestration that leaves behind a low carbon footprint and low earth temperature is desired to ameliorate climate change issues.[9] Previous suggestions involve technologies for capture and storage of CO_2 (CCS), but the cost of desorbing and compressing CO_2 from the capture solution to a potential CO_2 electrolyzer is a major challenge.[10,11] Instead of the CCS, electrochemical CO_2 capture and utilization emerge to eliminate storage costs and promote the generation of platform chemicals[12−17] and sustainable energy storage options.[18−21]

The electrochemical CO_2 reduction (ECO_2R) commonly uses CO_2 and amine solutions as inexpensive C-1 feedstock and electrolytes, respectively, to produce useful chemicals. For instance, the electroreduction of CO_2 to CO using ethylene diamine (EDA)/aqueous $NaClO_4$ electrolyte was reported to achieve Faradaic efficiency of 58% at the Cu electrode.[22] Similarly, monoethanolamine (MEA) electrolyte was reported to facilitate the ECO_2R to CO and $HCOO^-$, achieving 39.1 and 45% Faradaic efficiency, respectively. The low Faradaic efficiency is because the most captured CO_2 by MEA remained unused as free CO_2 approaches the Ag electrode in the amine electrolyte, unlike CO_2-rich carbamate species.[23] To control the ECO_2R by CO_2 adsorption or absorption, new stable electrolytes are required because the formation of protic substances by amines can limit the process.

Deep eutectic solvents (DESs) are promising as electrolytes for ECO_2R, as they are tunable for task-specific applications.[24−31] DESs are simple to prepare, requiring only the mixing of hydrogen bond donor (HBD) and hydrogen bond acceptor (HBA), avoiding any purification of side products.[32] So far, there are various cheap and renewable molecules that can serve as HBA or HBD, making DESs a potential and

Received: July 27, 2022
Accepted: September 26, 2022
Published: October 12, 2022

sustainable media for many applications. Because the HBA and HBD are joined by hydrogen bonds for DESs formation, charge delocalization is imminent, inducing distinct physicochemical features for high CO_2 solubility during ECO_2R application.[33−35] In accordance, non-amine-based DESs used as electrolyte for ECO_2R include choline chloride (ChCl) and urea-based DES in water (50 wt %)[36] and ChCl and ethylene glycol (EG)-based DES[37] over Ag electrode. These DESs electrolytes were able to facilitate CO_2 conversion to CO, achieving 96 and 78% Faradaic efficiency, respectively.

The amine-based DESs are only common for CO_2 capture,[38,39] but recently DESs such as methyl diethanolamine hydrochloride methyl diethanolamine (MDEAHCl-MDEA)[40] and zinc chloride ethanolamine (ZnCl-EA),[41] have facilitated ECO_2R to CO and $CO_2^{\bullet-}$, respectively. The MDEA stores CO_2 in the form of bicarbonate rather than carbamate, which has a higher theoretical CO_2-capturing capability than MEA.[42] Also the MDEAHCl have high CO_2 uptake[38,39] because of the high dielectric constant and basicity. These studies affirm the vaibility of amine-based deep eutectic solvents as electrolytes. As the amine-based deep eutectic electrolytes are emerging as media for ECO_2R, the consequent effect of double-layer capacitance (EDCL) structure in CO_2-saturated amine-based DESs is unclear. This EDCL is important to understand the interfacial phenomena during ECO_2R. Since some DESs are hydrophilic, water content associated with DESs as electrolytes could potentially induce hydrogen evolution reactions during ECO_2R. These challenges can collectively hamper the scalable development of effective DESs media as electrolyte for CO_2 electroreduction.[26,43]

This study investigates CO_2 electroreduction to $CO_2^{\bullet-}$ in novel diethylammonium chloride−diethanolamine (DEACl−DEA) ionic deep eutectic solvent as electrolyte. The ionic deep eutectic electrolyte was prepared from diethyl ammonium chloride (DEACl; HBA) and diethanolamine (DEA; HBD) and indexed as DEACl−DEA. The electrolyte was fully characterized to elucidate its physiochemical properties and stability that is suitable to enable understanding of interfacial phenomena during CO_2 saturation and electroreduction. Prior to the electroreduction process, the DEACl−DEA was vacuum dried to eliminate moisture that could induce hydrogen evolution reaction which reduces the energy efficiency of the CO_2 electroreduction process. Therefore, in the DEACl−DEA medium, the electroreduction of CO_2 to $CO_2^{\bullet-}$ was conducted in a membraneless electrolyzer. The corresponding current responses of $CO_2^{\bullet-}$ in DEACl−DEA were transformed to concentration for estimating the equivalent amount of CO_2 utilized during the process. The DEACl−DEA ionic deep eutectic electrolyte is unlike our previous study that used transition metal-based DESs with a pseudocapacitive attribute, in which case CO_2 saturation therein further increased the double layer capacitance.[41] Instead, DEACl−DEA has a different double layer capacitance features upon CO_2 saturation. Therefore, electrochemical impedance spectroscopy (EIS) in the potentiostatic mode elucidated the double layer structures in the CO_2-saturated ionic DEACl−DEA system during the electroreduction process at the CO_2−DEACl−DEA/Ag electrode interface. COSMO-RS theoretical analysis further elucidates the bifunctional attribute of DEACl−DEA, forming interaction with π-orbitals of CO_2 through its HBA and HBD sites. The work integrated several investigations to provide insights into CO_2 environments as well as a simple electrochemical method for assessing the gas processing and absorption capability of potential green solvents.

2. MATERIALS AND METHODS

2.1. Materials. Ultra-pure CO_2 and N_2 gas were purchased from Gaslink SDN Malaysia. DEA and DEACl were procured from Sigma-Aldrich, Darmstadt, Germany, having 98% purity. The fittings such as electrodes include counter electrode Pt wire/5.7 cm, BASi Inc., working electrode, silver (Ag)/OD: 6 mm, ID: 3 mm, and the reference electrode of Ag/AgCl (6 mm).

2.2. Preparation of DEACl−DEA. The ionic DESs were synthesized through constant mixing of known mole ratios (1:2, 1:3, 1:4, 1:5, and 1:6) of HBA (DEACl) and HBD (DEA) components at 70 °C for 8 h using a similar method reported previously.[32,41] Then, the DESs were dried and aged to observe the best mole ratio that maintained its fluidity without recrystallization.

2.3. Physiochemical Properties of DEACl−DEA. DSC-8000 PerkinElmer was used to assess the thermal behavior of the DEACl−DEA ionic DES sample. The experiments were carried out in a high-quality N_2 inert atmosphere of 20 mL min^{-1}. A sample of DEACl−DEA weighing less than 5 mg was partly encapsulated in aluminum pans to let the water evaporate freely. Multiple scans were carried out spanning the temperature range of 70−200 °C at cooling and heating speeds of 10 °C min^{-1}. The sample was held at 200 °C for a time after each scan to remove water. To get a stronger signal of the glass transition temperature, if present, and the melting point at the eutectic point, each sample was also held at 70 °C for 10 min.

The viscosity of DEACl−DEA ionic DESs was determined using a DV-II + Pro Extra Brookfield viscometer at 25 °C for different mole ratios similar to the previous report.[15] Typically, 10 mL of DEACl−DEA DES was poured into a cylindrical container immersed with the spindle. The spindle speed was set from the viscometer to different revolutions per minute (rpm) and corresponding shear rates (s^{-1}). Eventually, the viscosity of DEACl−DEA DES with different mole ratios was measured at ambient temperature throughout the process. A DM40 Mettler TOLEDO density meter was used to measure the density of DEACl−DEA ionic DESs across the temperature range of 25−90 °C in 10° steps.

2.4. Measurement of CO_2 Concentration in DEACl−DEA. The CO_2 solubility in ionic DESs was measured with the chronoamperometry module at −1.5 V *versus* Ag/AgCl similar to the previous procedure.[41] In a typical experiment, an electrochemical cell of 10 mL volume was filled to 1/4 capacity with dried ionic DESs and sparged with CO_2 at 5 bar, as illustrated in Figure S1. The electrochemical cell contains clamped Pt wire (5.7 cm, BASi Inc.) counter electrode, a silver (Ag) (OD: 6 mm, ID: 3 mm) working electrode, and a saturated Ag/AgCl (6 mm) reference electrode. The current response for CO_2 was recorded on an Auto-lab Potentiostat model PGSTAT302N. The cell containing saturated CO_2 was surrounded with N_2, while the measurement process proceeded for sterilization. Therefore, Nova 2.1 software was used to control data acquisition for detecting CO_2 solubility in the ionic DESs. During the process, 1 SCFH continuous CO_2 was maintained in the electrochemical cell for a maximum of 350 s stationary current value of I_∞ at 25 °C. The rates of CO_2 conversion through chemical absorption and dissolution are the same at I_∞ following a Cottrell-like chronoamperometry

https://doi.org/10.1021/acsomega.2c04739
ACS Omega 2022, 7, 37764−37773

profile with the onset of limiting currents of I_o that are momentarily transport controlled, as given by eq 1.[41] Concentration (C_o) of CO_2 was determined using eq 2, after substituting values of I_∞, I_o, A_1, and an equivalent weight of CO_2.

$$I = I_\infty + (I_o - I_\infty)\exp(-A_1 t) \quad (1)$$

$$C_o = I_o^2/[zFA_1\nu(I_o - I_\infty)] \quad (2)$$

$$I = \frac{nFAC_oD_o^{0.5}}{(\pi t)^{0.5}} = \left(\frac{nFAC_oD_o^{0.5}}{(\pi)^{0.5}}\right)\left(\frac{1}{(t)^{0.5}}\right) \quad (3)$$

$$\left(\frac{nFAC_oD_o^{0.5}}{(\pi)^{0.5}}\right) = \text{slope} \quad (4)$$

$$D_o = \left(\frac{\text{slope} \times (\pi)^{0.5}}{nFAC_o}\right)^2 \quad (5)$$

$$\text{FE}(\%) = \left(\frac{znF}{I \times t}\right) \times 100 \quad (6)$$

where I_∞ = stationary state current (mA/cm^2), I_{lim} = limiting current (mA/cm^2), C_o concentration (M) [equiv/cm^3, z = equivalent weight (g/equiv)], F= Faraday constant (96485.3 C mol^{-1}), ν = volume of electrolyte (mL). z = no. of electron, n = no. of CO_2 moles obtained from Ag electrode, I = total current (mA cm^{-2}), and t = time for a sample collection from the cell (s).

2.5. COSMO-RS Analysis of CO_2/DEACl−DEA Interaction. Using the graphical user interface of the Turbomole program version 4.0.,[15] the cut-out plane of DEACl−DEA DESs was constructed and optimized based on the Hartree−Fock level of theory and a def-SV (P) basis set. Then, utilizing density functional theory/Beck-Perdew-86 functional[15] and zeta valence potential (def-TZVP) basis set, a single-point calculation for the ionic DESs cut−off plane was carried out. Finally, to examine CO_2 interaction with the ionic DEACl−DEA DESs, a conductor-like screening model for realistic solvents (COSMO-RS) was employed based on BP-TZVP-C30-1401-CTD parameterization in COSMOthermX19 software.[44,45] To accurately characterize the ionic DESs, an electroneutral method was used in the COSMO-RS study. The CO_2 concentrations in ionic DESs were predicted using the solubility job function in COSMOTthermX19.

3. RESULTS AND DISCUSSION

3.1. Physicochemical Properties of DEACl−DEA. The DSC curve for DEACl−DEA in Figure 1a shows a shift of the baseline around −56.83 °C, indicating glass transition (T_g). Also, an endothermic peak was observed around −60.92 °C, indicating a melting transition. There is no exothermic peak for crystallization, indicating that DEACl−DEA is not in an amorphous state. The designation of DEACl−DEA as a glass former is made possible by the discovery of glass transition from which a glass transition temperature (T_g) value may be calculated. This is indicative of a shift in the DEACl−DEA's structure from a glass-like state to a rubber-like one, or vice versa, as shown by an increase in heat capacity. Consequently, the utilization of DEACl−DEA at the T_g for CO_2 capture application will not be viable. In Figure 1b, the eutectic point for DEACl−DEA occurs at a 1:3 mole ratio with the onset of

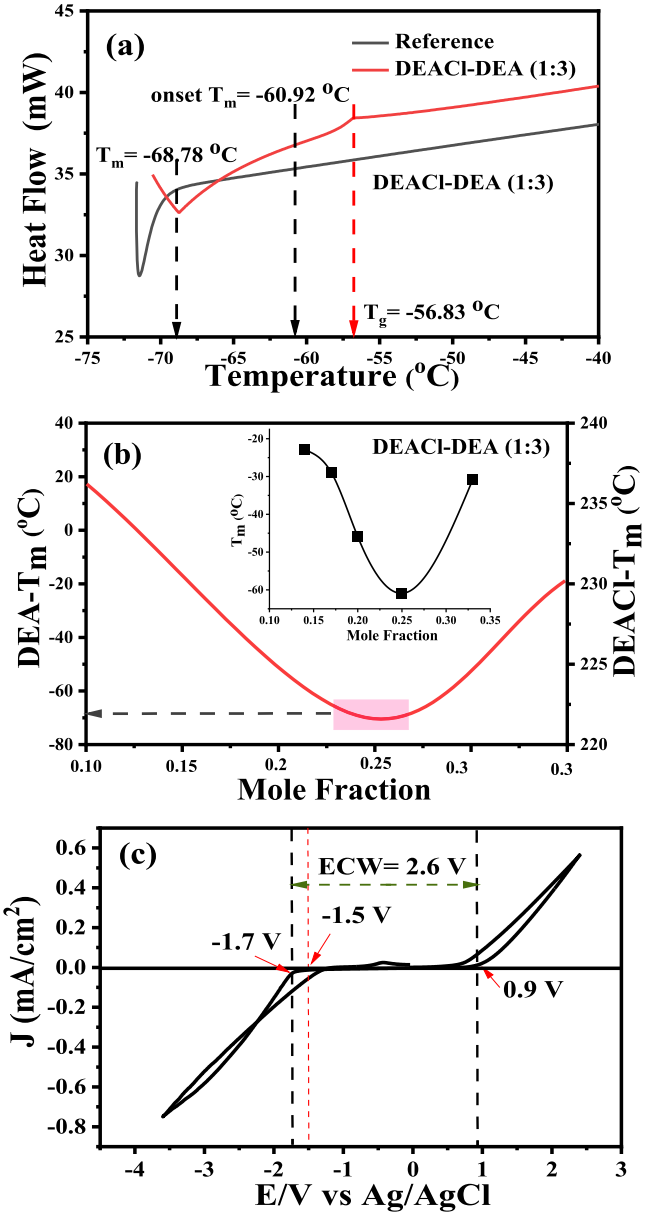

Figure 1. Physiochemical properties of DEACl−DEA: (a) DSC curve, (b) eutectic point, and (c) electrochemical stability window of DEACl−DEA.

−60.92 °C melting temperature until −68.78 °C. By heuristics, the DEACl−DEA is operable without melting up to 100 °C safe temperature, because over this temperature range (−70 to 100 °C), there is no thermal activity peak. Furthermore, following different mole ratios, DEACl−DEA have T_m = −68.78 °C lower than that of DEACl (T_m = 232 °C) and DEA (T_m = 28 °C). Common in the literature, the melting temperatures of some DESs are positive, but DEACl−DEA has a negative melting point similar to the zwitterionic DESs such as phenylacetic/betaine (2:1; T_m = −7 °C) and glycolic/betaine (2:1; T_m = −36 °C).[46] The negative melting point of DEACl−DEA or the zwitterionic DESs indicates that they can melt by liberating energy at the onset of melting without the requirement of any energy inputs. The effect of HBA/HBD mole fraction on the density of DEACl−DEA is shown in Table S1. The density of all the mole fractions was found to be ∼1.1 g/cm^3 to the nearest 1 decimal place similar to other

https://doi.org/10.1021/acsomega.2c04739
ACS Omega 2022, 7, 37764−37773

typical DESs reported previously. Moreover, the viscosity of DEACl−DEA shows that there is not much variation as the shear rate increases. This result is important for the continuous sparging of CO_2 in DEACl−DEA during the ECCO$_2$ process. Moreover, the stability of DEACl−DEA is an important feature to notice, particularly at the cathodic potential window of −1.7 V, as shown in Figure 2c. From −1.7 to 0.9 V, there is no observable Faradaic activity, implying that the electrochemical stability window is 2.6 V *versus* Ag/AgCl. Usually, DESs have a low electrochemical potential window,[35] but this result indicates the significance of cathodic limits for the prospective viability of DESs in electroreduction reactions similar to the previous report.[41]

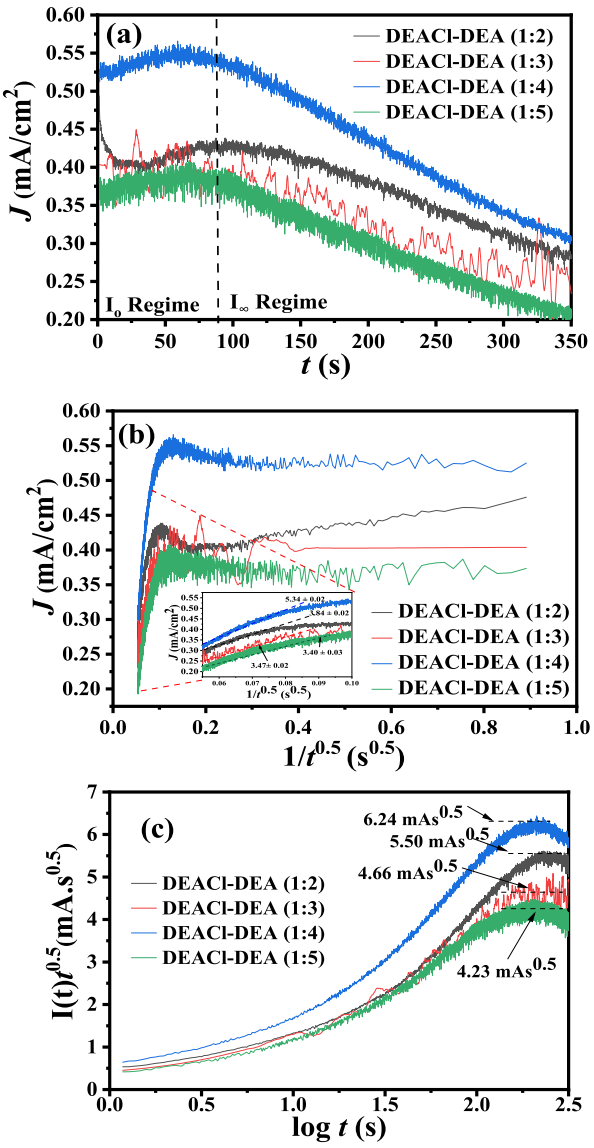

Figure 2. (a) Current response of CO_2 electroreduction in DEACl−DEA DES, (b) Cottrell diffusion current density *vs* $1/t^{0.5}$ for CO_2 electroreduction in DEACl−DEA DES, and (c) Cottrell diffusion in the form of the time dependence of the function $I(t)t^{0.5}$. The arrows define the maximum values of $I(t)t^{0.5}$, which are due to considerable Ohmic and kinetic resistive contributions to the total current.

3.2. Transient Current in CO_2 Saturated DEACl−DEA.

3.2.1. Limiting and Stationary Current Response. The current responses during CO_2 electroreduction in ionic DEACl−DEA are shown in Figure 2a. In screening the CO_2 capture capacity of DESs, estimating the current response is necessary. According to Figure 2a, during continuous sparging of CO_2 in the DESs, two prominent current patterns typical of the Cottrell-like profile, are recorded; (1) a current plateau (I_o), which later declined with time, and (2) a limiting current or stationary point where there are equal rates of CO_2 capture by the DESs and CO_2 conversion to $CO_2^{\bullet-}$, through chemical absorption. The onset potential for CO_2 reduction in DES of −1.0 and −1.5 V *versus* Ag/AgCl potential was adopted for CO_2 electroreduction to $CO_2^{\bullet-}$ free radical similar to the previous report.[41] For instance, CO_2−$CoCl_2$/EA had a 3.2 mA/cm^2 I_o-value and reached an I_∞-value of 1.4 mA/cm^2 after 700 s for CO_2 electroreduction to $CO_2^{\bullet-}$. In comparison, CO_2−DEACl−DEA have I_o-values of 0.432, 0.423, 0.566, and 0.38 mA/cm$_2$ for 1:2, 1:3, 1:4, and 1:5 mole ratios, respectively. The stationary current (I_∞-value) of 0.282, 0.267, 0.304, and 0.213 mA/cm$_2$ was reached during continuous CO_2 sparging into DEACl−DEA after 350 s. In a phenomenological sense, the swiftness in reaching a stationary state in the DEACl−DEA implies that there is high CO_2 coverage in the locality of the Ag working electrode. This current response, particularly reaching the stationary limit within 350 s, confirms the COSMO-RS suggestion of the bifunctional nature of DEACl−DEA in the physical capturing of CO_2 using its HBA (DEACl) and HBD (DEA) sites.

3.2.2. Rate-Determining Step. According to Figure 2b, the current response decreased with time during continuous sparging of CO_2 in DEACl−DEA to form the $CO_2^{\bullet-}$ free radical. Consequently, the onset period of the process where $t \approx 0$ and designated by I_o-regime diffusion, which is only high, may likely be the limiting step. In the I_o-regime, CO_2 consumption and conversion to $CO_2^{\bullet-}$ are not equal. The I_o-regime reaches a stationary current value of the I_∞-regime, where the rates of CO_2 consumption and conversion to $CO_2^{\bullet-}$ are equal. The values of CO_2 diffusion in DEACl−DEA DES are 3.130×10^{-10}, 2.822×10^{-10}, 8.352×10^{-10}, and 9.368×10^{-10} m^2/s, as computed from the Cottrell constant from Figure 2b. The Cottrell constant is a collection of parameters for the CO_2−DEACl−DEA DES system and varies for each mole ratio. For instance, the Cottrell constant for 1:2, 1:3, 1:4, and 1:5 mole ratio is 3.84 ± 0.02, 3.47 ± 0.02, 5.34 ± 0.02, and 3.40 ± 0.03, respectively. These Cottrell constant values were obtained from the slope according to eq 3, which is valid only for the finite-space diffusion in the short-time domain. However, the transition from the I_o-regime to the I_∞-regime is involved by long-time domain and the process may not be controlled only by the diffusion of CO_2. To confirm this observation, we investigate the short-time domain and compare it with the total time taken to reach I_∞-regime. The slopes of $I(t)$ *versus* $t^{-0.5}$ curves in the short-time domains were extrapolated to $t \approx 0$. This is the region where the short-time domain (τ_d) was estimated using L^2/D to be 3.478×10^{-10}, 3.859×10^{-10}, 1.304×10^{-10}, and 1.162×10^{-10} for CO_2 saturation in DEACl−DEA with mole ratios 1:2, 1:3, 1:4, and 1:5, respectively. These results are based on the CO_2 kinetic diameter of 0.330 nm[15] and the values of $\tau_d < I_\infty$-regime. The τ_d is very short in the nanosecond scale such that the process cannot only be diffusion controlled, but other limitations such as Ohmic drops or slow interfacial charge transfer kinetics could influence or be rate controlling during the transition from the I_o-regime to the I_∞-regime. As a result of using the traditional Cottrell equation to analyze transient current data,

https://doi.org/10.1021/acsomega.2c04739
ACS Omega 2022, 7, 37764−37773

the response of the working electrode cannot be attributed only to the diffusion control. Because Cottrell defines the current−time dependence for linear diffusion control, a linear relationship between i and $t^{-0.5}$ otherwise known as the Cottrell plot was expected. However, the linearity spans over only a short time (see the inset in Figure 2b), after which there is deviation. The deviation from the linearity of $i(t)$ *versus* $t^{-0.5}$ indicates electroreduction of CO_2 because −1.5 V is within the stable cathodic potential of DEACl−DEA. Overall, CO_2 diffusion, in addition to Ohmic drop or charge transfer resistance, might decide the step of CO_2 electroreduction. The plot of $i(t)t^{1/2}$*versus* log (t) in Figure 2c shows a maximum peak due to Ohmic drop and kinetic resistive contribution to the total current response for CO_2 reduction to $CO_2^{\bullet-}$.

3.3. Effect of *n*(DEACl)/*n*(DEA) on CO_2 Absorption and Electroreduction. Figure 3a shows the effect of the DEACl−DEA mole ratio on CO_2 physisorption. After continuous sparging of CO_2 into the DEACl−DEA, an observable increase in weight was recorded. The increase in weight of DEACl−DEA was attributed to the physisorption of CO_2 in the ionic media. The viscosity of DEACl−DEA also increased from 385 cP to 500 cP after sparging CO_2 continuously for 350 s, but the weight was a measure for easy referencing as shown in Figure 3a. By varying the mole ratios of DEACl−DEA during the pysisorption process, the mass transfer of CO_2 was adjusted relative to a unique equilibration time of the absorption process. In ordinaryDEA, the CO_2 capacity was only 0.05 μmol/L at 25 °C at ambient pressure after 350 s. However, in DEACl−DEA (1:3) DES, the physisorption capacity of CO_2 in the DEACl−DEA reaches up to 0.2 mol/L, minimum after 350 s of sparging (Figure 3a).

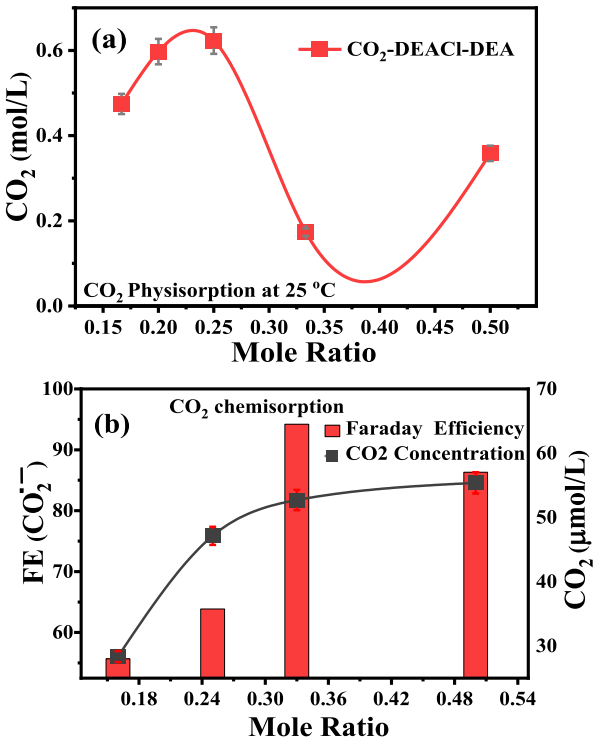

Figure 3. (a) Physisorption of CO_2 by DEACl−DEA. (b) Faraday efficiency of CO_2 electroreduction to $CO_2^{\bullet-}$ where the secondary axis shows the amount of CO_2 chemisorbed.

The chemisorption of CO_2 by DEACl−DEA was further investigated, where −1.5 V was supplied to the media. The results in Figure 3 b showed that different mole ratios of DEACl−DEA have unique CO_2 chemisorption. For instance, the mole capacity of CO_2 decreased from 52.7 μmol/L in DEACl−DEA DESs (1:3), which is the highest to 28.3 μmol/L in DEACl−DEA DESs (1:6). This is accompanied by the Faraday efficiency ($FECO_2^{\bullet-}$) increasing from 55 (DEACl−DEA; 1:6) to 95% (DEACl−DEA; 1:3) as the electrode was negatively polarized at −1.5 V in CO_2 saturated DEACl−DEA. Compared with previous studies, when MDEA used to produce MEAHCl-MDEA (1:4), the Faraday efficiency concerning producing CO was 71% at 1.1 V.[23,40] These Faraday efficiencies are different for CO_2 electroreduction to $CO_2^{\bullet-}$ in DEACl−DEA (1:3) as in the present study. Structurally, MDEA is different from DEA with the methyl group and a proton in the former and latter, respectively. Moreover, DEACl and MEAHCl are also different structurally in terms of two protons and a methyl group on the amine sites of the former and latter, respectively, with consequent different interactions with CO_2. Although CO_2 was converted in DEACl−DEA (1:3), the result therein is better than MEAHCl-MDEA (1:4) reported previously.

3.4. Effect of HBA and HBD on CO_2 Absorption and Electroreduction. The effect of HBA (TEACl or DEACl) and HBD (thymol or DEA) on CO_2 physisorption is shown in Figure 4a. After varying the mole fraction of HBA and HBD, TEACl−DEA was found to capture more CO_2 than DEACl-thymol. Compared with the data in Figure 4a, the amount of CO_2 captured by DEACl−DEA is also more than that captured by DEACl-thymol (1:4). By implication, the TEACl or DEACl

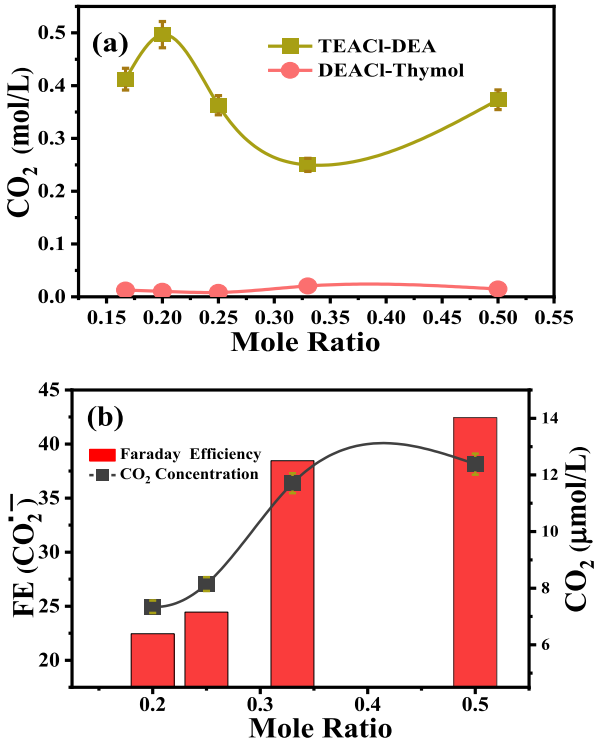

Figure 4. (a) Physisorption of CO_2 by DEACl-thymol and TEACl−DEA. (b) Faraday efficiency of CO_2 electroreduction to $CO_2^{\bullet-}$ in TEACl−DEA where the secondary axis shows the amount of CO_2 chemisorbed.

https://doi.org/10.1021/acsomega.2c04739
ACS Omega 2022, 7, 37764−37773

has a free amino group that can be used as an HBA to facilitate CO_2 capture below its critical pressure. On the contrary, thymol contains a phenolic hydroxyl group, which is suitable as an HBD. Previous studies found that when thymol was mixed with [TETA]Cl in a 1:3 mole ratio to form TETACl-thymol DES, thymol decreased the viscosity of TETACl.[47] Consequently, there was an improvement in the mass transfer of CO_2 in the absorbent, which lowered the time required to reach equilibrium. However, they found that thymol impedes the absorption capacity of CO_2, for instance, compared to ethylene glycol HBD.[48] Using TEPACl-thymol (1:3), the mole capacity of CO_2 was 1.339 mol CO_2/mol absorbent but decreased to 1.183 mol CO_2/mol absorbent upon increasing the amount of thymol to (1:7). In congruence with previous investigations, the addition of acidic components in ionic or non-ionic solvents potentially lowers the capacity of acidic gases.[49,50] This is considering that thymol is weakly acidic due to likely deprotonation from its phenolic group.[47] As a result, acidic attributes of thymol could decrease the capacity of CO_2 in DESs.

Figure 4b shows the chemisorption of CO_2 on TEACl−DEA through CO_2 electroreduction. The primary axis is the Faradaic efficiency for CO_2 electroreduction to $CO_2^{\bullet-}$. The secondary axis shows the CO_2 absorption capacity. The TEACl−DEA (1:2) electrolyte gave the best Faradaic efficiency for CO_2 electroreduction to $CO_2^{\bullet-}$ (42.5%). Also, the CO_2 absorption capacity of 12.4 μmol/L was obtained due to chemisorption is best in TEACl−DEA (1:2). We established that the DEACl-thymol is not electrochemically stable as there is no observable electrochemical window. Consequently, the CO_2 electroreduction in DEACl-thymol is not assured to only CO_2 but also to DEACl-thymol electrolyte components such as DEACl or thymol.

3.5. COSMO-RS Analysis of CO_2-Ionic DESs Interaction. The COSMO-RS analysis is significant to confirm CO_2 absorption by the ionic DESs, which ensures its high coverage near the surface of the working electrode. High coverage of CO_2 at the surface of the electrode assures the generation of $CO_2^{\bullet-}$ free radical.[41] As a result, the ionic DEACl−DEA DES captures the CO_2 through non-covalent interactions, and the coverage can be high at the electrode surface. Using σ-profiles, the screening charge density of the ionic DESs was used to assess their non-covalent interaction with CO_2. The respite peaks in the ionic DEACl−DEA DES's σ-profile are shown in Figure 5a at 1.677, 0.013, and 0.567 e/nm^2 at the DEACl site and 1.677, 0.115, 0.396, 1.277, and 1.730 e/nm^2 at the DEA screening charge density. Similar respite peaks can be seen in the σ-profile of CO_2 at 0.598, 0.314, 0.097, and 0.779 e/nm^2. The non-polar contribution region, where I_o-values are between 1.0 and +1.0 e/nm^2, is where the DEACl−DEA DES and CO_2 interacting screening charge densities are located.[51,52] As previously reported,[41] the screening charge densities on linear-symmetric CO_2's electron function can indicate the non-polar contribution of linear−CO_2 interaction with DESs, including ionic DES. It is worth noting that the CO_2 interaction with DEACl−DEA DES is not the form of energized CO_2 ($CO_2^{\bullet-}$ free radical) with geometry from linear to bent at ∼150°.[41,53] The interaction of CO_2 with DEACl−DEA DES based on the COSMO-RS analysis occurs on their non-polar sites such as −0.013, −0.567 e/nm^2 at the DEACl site and −0.314, −0.097, −0.779 e/nm^2 on CO_2. Moreover, the 0.115, −0.396 e/nm^2 non-polar site on DEA can interact with −0.314, −0.097, −0.779 e/nm^2 on CO_2. The

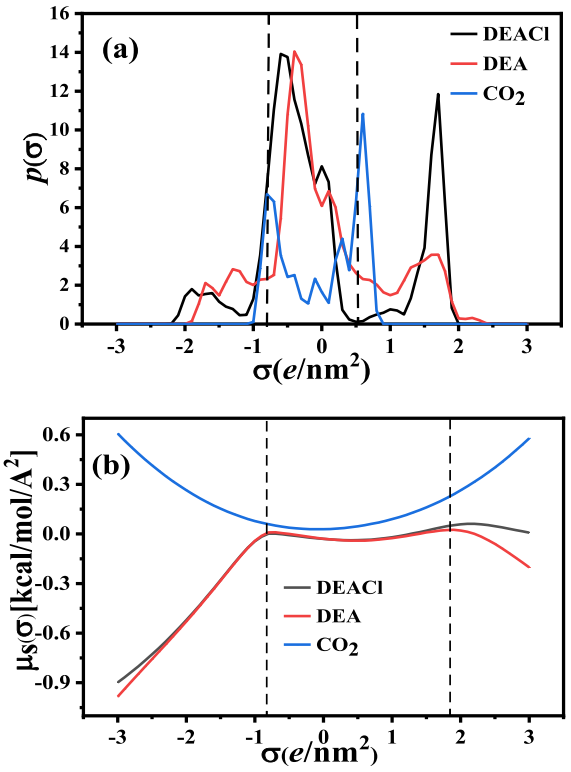

Figure 5. COSMO-RS analysis showing (a) σ-profiles of DEACl−DEA DES and (b) σ-potential of DEACl−DEA DES.

results also confirmed that the interaction of CO_2 with the ionic DES occurs in the non-polar region similar to the transition metal-based DESs reported previously.[41] The DEACl−DEA DES has bifunctional attributes as both the HBD and HBA have been indicated by COSMO-RS analysis to interact with neutral CO_2. These interactions are based on the criterion of like dissolves like. This indicates that the less endothermic the enthalpy of the solution is, the more soluble CO_2 is in ionic DESs, and vice versa.

As illustrated in Figure 5b, the σ-potential, which is the plot of surface chemical potentials of DEACl−DEA DES or CO_2 as a function of screening charge density, was also measured. The negative polarity is connected with a significantly negative σ-potential charge density of more than 1.1 or 2.245 e/nm^2. This demonstrates that DEACl or DEA has an electron donor property, causing hydrogen to interact with the exposed oxygen atoms from the hydroxyl, nitrogen in the amine in DEA, or chlorine ends in DEACl. CO_2 exhibits a positive potential at charge densities larger than 1−2 e/nm^2, indicating that it possesses electron-accepting characteristics.

The σ-potential, which is the plot of surface chemical potentials of DEACl−DEA DES or CO_2 as a function of screening charge density, was also determined as shown in Figure 5b. The highly negative σ-potential charge density greater than −1.1 or 2.245 e/nm^2 is associated with negative polarity. This shows that DEACl or DEA has an electron donor property, which causes hydrogen to interact with the exposed oxygen atoms from the hydroxyl, nitrogen in the amine in DEA, or chlorine ends in DEACl. For charge densities greater than −1 or 2 e/nm^2, CO_2 has a positive σ-potential, showing that it has electron-accepting properties. DEACl−DEA display dual chemical potentials larger than 0.931 e/nm^2, indicating an electron-donating property with negative chemical potential

https://doi.org/10.1021/acsomega.2c04739
ACS Omega 2022, 7, 37764−37773

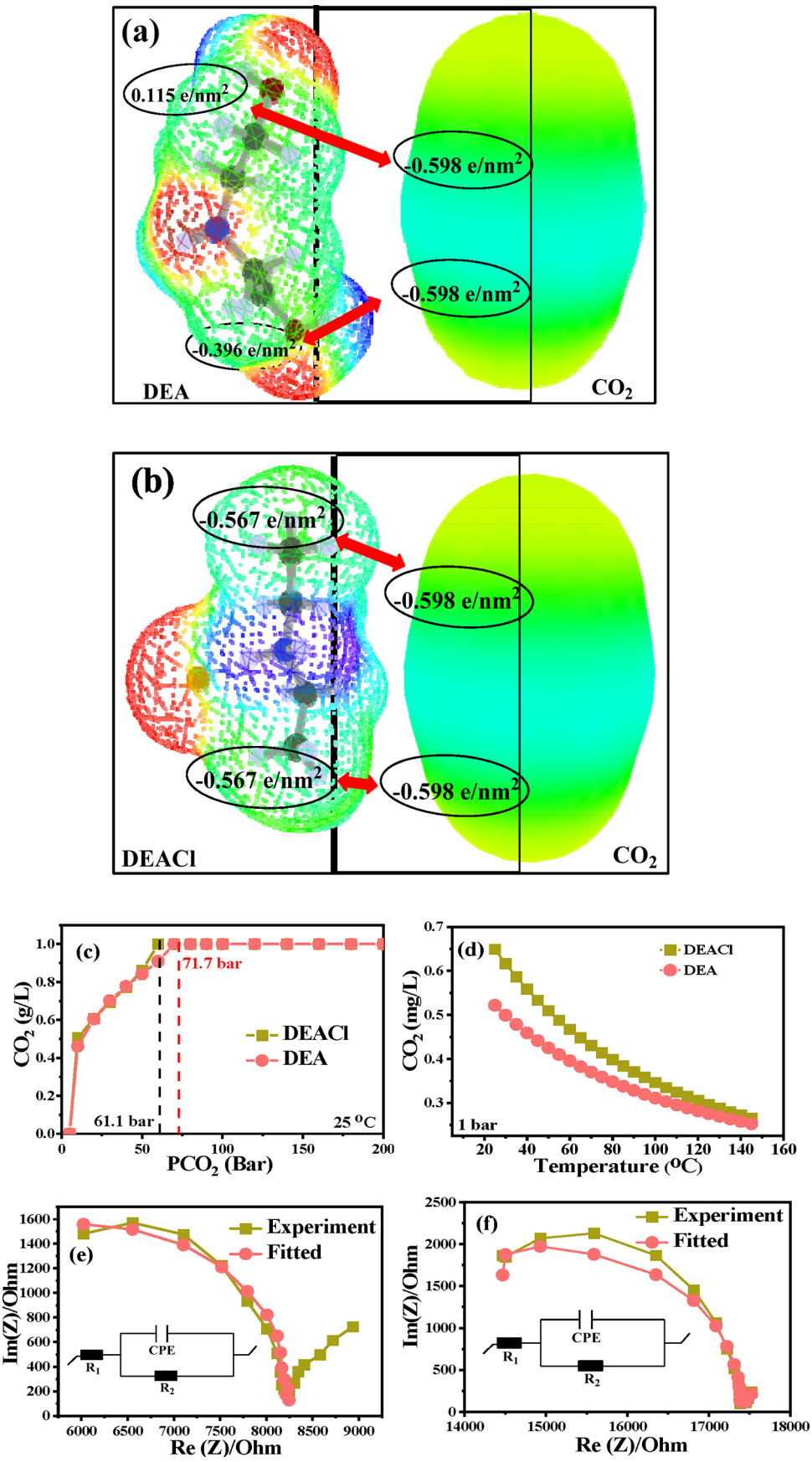

Figure 6. (a) Sigma surface showing the interaction of DEA with CO_2, (b) sigma surface showing the interaction of DEACl with CO_2, (c) effect of pressure on COSMO-RS CO_2 solubility at DEA and DEACl sites, (d) effect of temperature on COSMO-RS CO_2 solubility at DEA and DEACl sites, (e) Nyquist plot for ordinary DEACl–DEA, and (f) Nyquist plot for CO_2 saturated DEACl–DEA.

https://doi.org/10.1021/acsomega.2c04739
ACS Omega 2022, 7, 37764–37773

Table 1. EIS Characteristics for ECO_2R at −1.5 V *Versus* Ag/AgCl under Normal and CO_2 Saturation Conditions at Ag Electrode

S/N	ionic deep eutectic electrolyte	R_s (Ohm)	R_{ct} (Ohm)	C_{dl} (nF)	μ (cP)	ρ (g/cm^{-3})
1	DEACl−DEA	3,815	348.6	8.759	401.9	1.09
2	CO_2−DEACl−DEA	12,756	809.3	3.145	528.5	2.03

for DEACl and DEA sites. These findings support the notion that neutral CO_2 absorbed via the HBA or HBD site in ionic DESs is more likely to form CO_2 free radicals during the CO_2 electroreduction process.

3.6. Mechanism of CO_2 Absorption and Electroreduction in DEACl−DEA. COSMO-RS sigma profile analysis (Figure 5a,b), COSMO surface (Figure 6a,b), and CO_2 physisorption or solubility were used to determine and understand the bifunctional way of delivering CO_2 to the electrode in DEACl−DEA electrolyte (Figure 6c,d). According to the COSMO-RS study, the DEACl−DEA ionic DES can capture a considerable quantity of CO_2 even at low CO_2 partial pressures until a critical pressure of 61 and 71.7 bar is attained at the DEACl and DEA sites, respectively (see Figure 6c,d). The high capacity of CO_2 in DEACl−DEA DES reveals that DEACl−DEA and CO_2 interact not only physically but also chemically. Furthermore, as indicated in Table 1, the density, viscosity, and mass of DEACl−DEA increased following CO_2 absorption. This means that new interacting bonds were formed during CO_2 absorption, with the chemical interaction being substantially stronger than the physical relationship. On their COSMO surface, the physical interaction between CO_2 and DEACl−DEA is depicted in Figure 6a for DEACl and Figure 6b for the DEA site.

EIS was utilized to confirm the chemisorption of CO_2 by DEACl−DEA electrolyte. The Nyquist curve for impedance measurement in DEACl−DEA under −1.5 V potentiostatic control before and after CO_2 absorption was measured and is shown in Figure 6e and f, respectively. The difference in Nyquist plot response in DEACl−DEA before and after CO_2 sparging suggests changes in the interfacial double layer capacitance structure of the ionic DEACl−DEA DES with CO_2. The DEACl−DEA system's Nyquist plot (Figure 6e) has a smaller semicircle than the CO_2−DEACl−DEA system (Figure 6f and Table 1). When regular DEACl−DEA was compared to CO_2−DEACl−DEA, this result indicated faster charge transfer processes with resistive-capacitive (RC) circuits.

The equivalent circuit (EC) illustrated in the insets of Figure 6e and f were used to estimate impedance parameters (see Table 1) such as capacitance in conjunction with the RC circuit of the Nyquist plot for DEACl−DEA or CO_2−DEACl−DEA systems. The EC was designed with two resistances R_1 and R_2 as well as a double layer capacitance inform of constant phase element. The resistance of the DEACl−DEA or CO_2−DEACl−DEA medium is R_1, and the resistance of the interfacial charge transfer necessary for CO_2 electroreduction to CO_2 free radical is R_2. As a result, it was discovered that the resistance (R_1) of DEACl−DEA media is 3815 and 12756 Ω for CO_2−DEACl−DEA media. The rise in medium resistance following CO_2 sparging in DEACl−DEA seems to indicate the media's CO_2 sorption capability. According to Figure 6e, the capacitance of the DEACl−DEA medium is 8.759 nF before sparging CO_2, with a Faradaic charge transfer resistance of 348.6 Ω. Furthermore, after sparging CO_2, the capacitance of the CO_2−DEACl−DEA medium reduced to 3.145 nF, with a Faradaic charge transfer resistance of 809.3 Ω. This reduction in interfacial capacitance in DEACl−DEA with CO_2 saturation raises the mechanistic possibility that CO_2 chemically binds to the DEACl and DEA sites. After physical absorption, CO_2 electroreduction is achievable at −1.5 V *versus* Ag/AgCl; however. when electrochemically reduced to $CO_2^{\bullet-}$, it bonds without generating any ionic specie that would contribute to the double layer.

This CO_2 behavior in DEACl−DEA ionic DES differs from that seen in the transition metal DES class of ionic DESs. We previously discovered that the CO_2 behavior in TDES necessitates the presence of ionic species such as $CO_2^{\bullet-}$ from CO_2, $C_3H_5O_4^-$ (zwitterions) from R-NH_2 functionality, or $-RCO_3^{2-}$ (carbonate ion) from R−OH functionality in the double layer at the Ag electrode surface.[41] Furthermore, by setting the EIS measurement to −1.5 V *versus* Ag/AgCl, the CO_2 undergoes electroreduction while the ionic DEACl−DEA medium remains unlikely to form ions at the compact layer. There is a strong likelihood that the $CO_2^{\bullet-}$ produced in the diffuse layer (outer Helmholtz plane) will bind to the DEACl and DEA sites.

As a result, because the ionic DEACl−DEA forms a continuous phase, they are confined, and the current response produced results from scattered CO_2 electroreduction to $CO_2^{\bullet-}$ free radical. To enhance electron transport to CO_2, Ag^+ forms the inner Helmholtz plane (see Figure S2). When the DEACl−DEA is saturated with CO_2, the double layer capacitance decreases. Because the $CO_2^{\bullet-}$ created binds with the DES, the ionic species after saturating DEACl−DEA with CO_2 is most likely solely the Ag^+ surface. To confirm this discovery, free DEACl−DEA was measured using EIS, and the double layer capacitance was shown to be greater.

4. CONCLUSIONS

The activity of amine-based bifunctional ionic deep eutectic electrolytes for CO_2 electroreduction was demonstrated in this study. Because amine-based ionic deep eutectic electrolytes do not have pseudocapacitive properties, saturating them with CO_2 suppresses the interfacial double layer capacitance. Further investigation revealed that the types of HBD and HBA used, as well as their molar ratios, can affect CO_2 reduction performance. Moreover, HBA with longer chain length can reduce the Faradaic efficiency of CO_2 electroreduction in ionic DESs. DEACl, which has a short chain length, demonstrated 71% Faraday efficiency for CO_2 electroreduction to $CO_2^{\bullet-}$. This is in contrast to TEACl, which has a longer chain length and achieved a Faradaic efficiency of 38.6% for CO_2 electroreduction to CO_2. Most importantly, the DEACl−DEA have a higher cathodic electrochemical stability limit than the typical potential required to electrochemically reduce CO_2, indicating that the process of reducing CO_2 in deep eutectic electrolyte is feasible. These findings open up the possibility of stabilizing amine via the formation of deep eutectic electrolytes for long-term CO_2 capture and electroreduction.

https://doi.org/10.1021/acsomega.2c04739
ACS Omega 2022, 7, 37764−37773

■ ASSOCIATED CONTENT

Supporting Information

The Supporting Information is available free of charge at https://pubs.acs.org/doi/10.1021/acsomega.2c04739.

Experimental setup for CO_2 electroreduction in DEACl−DEA, flow properties of DEACl−DEA at ambient condition, and interfacial depiction of CO_2 reduction in DEACl−DEA electrolyte (PDF)

■ AUTHOR INFORMATION

Corresponding Authors

Ahmed Halilu − *Department of Chemical Engineering, Faculty of Engineering, University of Malaya, Kuala Lumpur 50603, Malaysia; University of Malaya Centre for Ionic Liquids (UMCiL), University of Malaya, Kuala Lumpur 50603, Malaysia;* orcid.org/0000-0003-0381-2365; Email: ahmed_h@um.edu.my

Mohamed Kamel Hadj-Kali − *Chemical Engineering Department, College of Engineering, King Saud University, Riyadh 11421, Saudi Arabia;* orcid.org/0000-0002-1374-9825; Email: mhadjkali@ksu.edu.sa

Authors

Mohd Ali Hashim − *Department of Chemical Engineering, Faculty of Engineering, University of Malaya, Kuala Lumpur 50603, Malaysia; University of Malaya Centre for Ionic Liquids (UMCiL), University of Malaya, Kuala Lumpur 50603, Malaysia*

Rozita Yusoff − *Department of Chemical Engineering, Faculty of Engineering, University of Malaya, Kuala Lumpur 50603, Malaysia;* orcid.org/0000-0003-1654-4478

Mohamed Kheireddine Aroua − *Centre for Carbon Dioxide Capture and Utilisation (CCDCU), School of Science and Technology and Sunway Materials Smart Science & Engineering Research Cluster (SMS2E), Sunway University, Petaling Jaya 47500, Malaysia; School of Engineering, Lancaster University, Lancaster LA1 4YW, U.K.;* orcid.org/0000-0002-9388-5439

Complete contact information is available at: https://pubs.acs.org/10.1021/acsomega.2c04739

Notes

The authors declare no competing financial interest.

■ ACKNOWLEDGMENTS

Dr. HADJ-KALI would like to express his appreciation to the Researchers Supporting Project (RSP-2021/361), King Saud University, Riyadh, Saudi Arabia, for the financial support throughout this research.

■ REFERENCES

(1) Hashimoto, K.Global temperature and atmospheric carbon dioxide concentration. In *Global Carbon Dioxide Recycling*; Springer, 2019; pp 5−17.

(2) NOAACarbon dioxide peaks near 420 parts per million at Mauna Loa observatory. 2021, https://research.noaa.gov/article/ArtMID/587/ArticleID/2764 (accessed July 6, 2021).

(3) Benson, S. M.; Orr, F. M. Carbon dioxide capture and storage. *MRS Bull.* **2008**, *33*, 303−305.

(4) Leung, D. Y.; Caramanna, G.; Maroto-Valer, M. M. An overview of current status of carbon dioxide capture and storage technologies. *Renew. Sustain. Energy Rev.* **2014**, *39*, 426−443.

(5) Meckling, J.; Biber, E. A policy roadmap for negative emissions using direct air capture. *Nat. Commun.* **2021**, *12*, 2051.

(6) Tollefson, J. Sucking carbon dioxide from air is cheaper than scientists thought. *Nature* **2018**, *558*, 173.

(7) UNFCCC, V.Adoption of the Paris agreement. 2022, https://unfccc.int/process-and-meetings/the-paris-agreement/the-paris-agreement (accessed June 6, 2022).

(8) Wilcox, J.; Haghpanah, R.; Rupp, E. C.; He, J.; Lee, K. Advancing adsorption and membrane separation processes for the gigaton carbon capture challenge. *Annu. Rev. Chem. Biomol. Eng.* **2014**, *5*, 479−505.

(9) Müller, L. J.; Kätelhön, A.; Bringezu, S.; McCoy, S.; Suh, S.; Edwards, R.; Sick, V.; Kaiser, S.; Cuéllar-Franca, R.; El Khamlichi, A.; Lee, J. H.; von der Assen, N.; Bardow, A. The carbon footprint of the carbon feedstock CO_2. *Energy Environ. Sci.* **2020**, *13*, 2979−2992.

(10) Chadwick, A.; Smith, D.; Hodrien, C.; Hovorka, S.; Mackay, E.; Mathias, S.; Lovell, B.; Kalaydjian, F.; Sweeney, G.; Benson, S.; Dooley, J.; Davidson, C. The realities of storing carbon dioxide—A response to CO_2 storage capacity issues raised by Ehlig-Economides & Economides. *Nat. Preced.* **2010**, DOI: 10.1038/npre.2010.4500.1.

(11) Sorimachi, K. Innovative method for CO_2 fixation and storage. *Sci. Rep.* **2022**, *12*, 1694.

(12) Peterson, A. A.; Abild-Pedersen, F.; Studt, F.; Rossmeisl, J.; Nørskov, J. K. How copper catalyzes the electroreduction of carbon dioxide into hydrocarbon fuels. *Energy Environ. Sci.* **2010**, *3*, 1311−1315.

(13) Kim, T.; Palmore, G. T. R. A scalable method for preparing Cu electrocatalysts that convert CO_2 into C^{2+} products. *Nat. Commun.* **2020**, *11*, 3622.

(14) Fan, L.; Xia, C.; Zhu, P.; Lu, Y.; Wang, H. Electrochemical CO_2 reduction to high-concentration pure formic acid solutions in an all-solid-state reactor. *Nat. Commun.* **2020**, *11*, 3633.

(15) Halilu, A.; Hayyan, M.; Aroua, M. K.; Yusoff, R.; Hizaddin, H. F. In Situ Electrosynthesis of Peroxydicarbonate Anion in Ionic Liquid Media Using Carbon Dioxide/Superoxide System. *ACS Appl. Mater. Interfaces* **2019**, *11*, 25928−25939.

(16) Halilu, A.; Hayyan, M.; Aroua, M. K.; Yusoff, R.; Hizaddin, H. F. Mechanistic insights into carbon dioxide utilization by superoxide ion generated electrochemically in ionic liquid electrolyte. *Phys. Chem. Chem. Phys.* **2021**, *23*, 1114−1126.

(17) Halilu, A.; Hayyan, M.; Aroua, M. K.; Yusoff, R.; Hizaddin, H. F.; Basirun, W. J. Hybridized Fe/Ru-SiMWCNT-ionic liquid nanofluid for CO_2 conversion into carbamate using superoxide ion. *J. Environ. Chem. Eng.* **2021**, *9*, 105285.

(18) Paz-Garcia, J. M.; Dykstra, J.; Biesheuvel, P.; Hamelers, H. Energy from CO_2 using capacitive electrodes - A model for energy extraction cycles. *J. Colloid Interface Sci.* **2015**, *442*, 103−109.

(19) Hamelers, H.; Schaetzle, O.; Paz-García, J.; Biesheuvel, P.; Buisman, C. Harvesting Energy from CO_2 Emissions. *Environ. Sci. Technol. Lett.* **2014**, *1*, 31−35.

(20) Stevens, G. B.; Reda, T.; Raguse, B. Energy storage by the electrochemical reduction of CO_2 to CO at a porous Au film. *J. Electroanal. Chem.* **2002**, *526*, 125−133.

(21) Wang, F.; Li, Y.; Xia, X.; Cai, W.; Chen, Q.; Chen, M. Metal-CO_2 Electrochemistry: From CO_2 Recycling to Energy Storage. *Adv. Energy Mater.* **2021**, *11*, 2100667.

(22) Abdinejad, M.; Mirza, Z.; Zhang, X.-a.; Kraatz, H.-B. Enhanced Electrocatalytic Activity of Primary Amines for CO_2 Reduction Using Copper Electrodes in Aqueous Solution. *ACS Sustainable Chem. Eng.* **2020**, *8*, 1715−1720.

(23) Chen, L.; Li, F.; Zhang, Y.; Bentley, C. L.; Horne, M.; Bond, A. M.; Zhang, J. Electrochemical reduction of carbon dioxide in a monoethanolamine capture medium. *ChemSusChem* **2017**, *10*, 4109−4118.

(24) Zhang, N.; Huang, Z.; Zhang, H.; Ma, J.; Jiang, B.; Zhang, L. Highly Efficient and Reversible CO_2 Capture by Task-Specific Deep Eutectic Solvents. *Ind. Eng. Chem. Res.* **2019**, *58*, 13321−13329.

(25) Sze, L. L.; Pandey, S.; Ravula, S.; Pandey, S.; Zhao, H.; Baker, G. A.; Baker, S. N. Ternary deep eutectic solvents tasked for carbon dioxide capture. *ACS Sustainable Chem. Eng.* **2014**, *2*, 2117−2123.

(26) Smith, E. L.; Abbott, A. P.; Ryder, K. S. Deep eutectic solvents (DESs) and their applications. *Chem. Rev.* **2014**, *114*, 11060−11082.
(27) Wazeer, I.; Hadj-Kali, M. K.; Al-Nashef, I. M. Utilization of deep eutectic solvents to reduce the release of hazardous gases to the atmosphere: A critical review. *Molecules* **2021**, *26*, 75.
(28) Ali, E.; Hadj-Kali, M. K.; Mulyono, S.; Alnashef, I. Analysis of operating conditions for CO_2 capturing process using deep eutectic solvents. *Int. J. Greenh. Gas Control* **2016**, *47*, 342−350.
(29) Isik, M.; Zulfiqar, S.; Edhaim, F.; Ruiperez, F.; Rothenberger, A.; Mecerreyes, D. Sustainable Poly(Ionic Liquids) for CO_2 Capture Based on Deep Eutectic Monomers. *ACS Sustainable Chem. Eng.* **2016**, *4*, 7200−7208.
(30) Yang, X.; Zou, Q.; Zhao, T.; Chen, P.; Liu, Z.; Liu, F.; Lin, Q. Deep Eutectic Solvents as Efficient Catalysts for Fixation of CO2 to Cyclic Carbonates at Ambient Temperature and Pressure through Synergetic Catalysis. *ACS Sustainable Chem. Eng.* **2021**, *9*, 10437−10443.
(31) Song, Z.; Hu, X.; Wu, H.; Mei, M.; Linke, S.; Zhou, T.; Qi, Z.; Sundmacher, K. Systematic Screening of Deep Eutectic Solvents as Sustainable Separation Media Exemplified by the CO_2 Capture Process. *ACS Sustainable Chem. Eng.* **2020**, *8*, 8741−8751.
(32) Abbott, A. P.; Harris, R. C.; Ryder, K. S.; D'Agostino, C.; Gladden, L. F.; Mantle, M. D. Glycerol eutectics as sustainable solvent systems. *Green Chem.* **2011**, *13*, 82−90.
(33) Cao, L.; Huang, J.; Zhang, X.; Zhang, S.; Gao, J.; Zeng, S. Imidazole tailored deep eutectic solvents for CO_2 capture enhanced by hydrogen bonds. *Phys. Chem. Chem. Phys.* **2015**, *17*, 27306−27316.
(34) Zahn, S.; Kirchner, B.; Mollenhauer, D. Charge spreading in deep eutectic solvents. *ChemPhysChem* **2016**, *17*, 3354−3358.
(35) Smith, E. L.; Abbott, A. P.; Ryder, K. S. Deep Eutectic Solvents (DESs) and Their Applications. *Chem. Rev.* **2014**, *114*, 11060−11082.
(36) Garg, S.; Li, M.; Rufford, T. E.; Ge, L.; Rudolph, V.; Knibbe, R.; Konarova, M.; Wang, G. G. X. Catalyst-Electrolyte Interactions in Aqueous Reline Solutions for Highly Selective Electrochemical CO_2 Reduction. *ChemSusChem* **2020**, *13*, 304−311.
(37) Vasilyev, D. V.; Rudnev, A. V.; Broekmann, P.; Dyson, P. J. A general and facile approach for the electrochemical reduction of carbon dioxide inspired by deep eutectic solvents. *ChemSusChem* **2019**, *12*, 1635−1639.
(38) Bi, Y.; Hu, Z.; Lin, X.; Ahmad, N.; Xu, J.; Xu, X. Efficient CO_2 capture by a novel deep eutectic solvent through facile, one-pot synthesis with low energy consumption and feasible regeneration. *Sci. Total Environ.* **2020**, *705*, 135798.
(39) Trivedi, T. J.; Lee, J. H.; Lee, H. J.; Jeong, Y. K.; Choi, J. W. Deep eutectic solvents as attractive media for CO_2 capture. *Green Chem.* **2016**, *18*, 2834−2842.
(40) Ahmad, N.; Wang, X.; Sun, P.; Chen, Y.; Rehman, F.; Xu, J.; Xu, X. Electrochemical CO_2 reduction to CO facilitated by MDEA-based deep eutectic solvent in aqueous solution. *Renewable Energy* **2021**, *177*, 23−33.
(41) Halilu, A.; Hadj-Kali, M. K.; Hashim, M. A.; Ali, E. M.; Bhargava, S. K. Electroreduction of CO_2 and Quantification in New Transition-Metal-Based Deep Eutectic Solvents Using Single-Atom Ag Electrocatalyst. *ACS Omega* **2022**, *7*, 14102−14112.
(42) El Hadri, N.; Quang, D. V.; Goetheer, E. L. V.; Abu Zahra, M. R. M. Aqueous amine solution characterization for post-combustion CO_2 capture process. *Appl. Energy* **2017**, *185*, 1433−1449.
(43) Zhang, Q.; De Oliveira Vigier, K.; Royer, S.; Jérôme, F. Deep eutectic solvents: syntheses, properties and applications. *Chem. Soc. Rev.* **2012**, *41*, 7108−7146.
(44) Hornig, M.; Klamt, A. COSMOfrag: A novel tool for high-throughput adme property prediction and similarity screening based on quantum chemistry. *J. Chem. Inf. Model.* **2005**, *45*, 1169−1177.
(45) Ali, E.; Hadj-Kali, M. K.; Alnashef, I. Modeling of CO_2 Solubility in Selected Imidazolium-Based Ionic Liquids. *Chem. Eng. Commun.* **2017**, *204*, 205−215.
(46) Cardellini, F.; Tiecco, M.; Germani, R.; Cardinali, G.; Corte, L.; Roscini, L.; Spreti, N. Novel zwitterionic deep eutectic solvents from trimethylglycine and carboxylic acids: characterization of their properties and their toxicity. *RSC Adv.* **2014**, *4*, 55990−56002.
(47) Gu, Y.; Hou, Y.; Ren, S.; Sun, Y.; Wu, W. Hydrophobic Functional Deep Eutectic Solvents Used for Efficient and Reversible Capture of CO_2. *ACS Omega* **2020**, *5*, 6809−6816.
(48) Zhang, K.; Hou, Y.; Wang, Y.; Wang, K.; Ren, S.; Wu, W. Efficient and Reversible Absorption of CO_2 by Functional Deep Eutectic Solvents. *Energy Fuels* **2018**, *32*, 7727−7733.
(49) Ren, S.; Hou, Y.; Wu, W.; Jin, M. Oxidation of SO_2 Absorbed by an Ionic Liquid during Desulfurization of Simulated Flue Gases. *Ind. Eng. Chem. Res.* **2011**, *50*, 998−1002.
(50) Wu, Z.; Hou, Y.; Wu, W.; Ren, S.; Zhang, K. Efficient Removal of Sulfuric Acid from Sodium Lactate Aqueous Solution Based on the Common-Ion Effect for the Absorption of SO_2 of Flue Gas. *Energy Fuels* **2019**, *33*, 4395−4400.
(51) Klamt, A.; Eckert, F.; Arlt, W. COSMO-RS: An Alternative to Simulation for Calculating Thermodynamic Properties of Liquid Mixtures. *Annu. Rev. Chem. Biomol. Eng.* **2010**, *1*, 101−122.
(52) Eckert, F.; Klamt, A.*COSMOtherm*. Version C2, 2013; p 1.
(53) Gutsev, G. L.; Bartlett, R. J.; Compton, R. N. Electron affinities of CO_2, OCS, and CS_2. *J. Chem. Phys.* **1998**, *108*, 6756−6762.

https://doi.org/10.1021/acsomega.2c04739
ACS Omega 2022, 7, 37764−37773